Facile Electrodeposition of Ti_5Si_3 Films from Oxide Precursors in Molten $CaCl_2$

WEI TANG, GUANGSHI LI, ZHONGYA PANG, XIANGYU XU, KAI ZHU, QIAN XU, XINGLI ZOU, and XIONGGANG LU

It is hard to produce dense refractory Ti_5Si_3 films at low temperature because of the extremely high melting point (2130 °C) of Ti_5Si_3. Herein, we report the facile electrodeposition of Ti_5Si_3 films from TiO_2 and SiO_2 in molten $CaCl_2$-CaO at 850 °C. Crystalline Ti_5Si_3 films with tunable film thicknesses and morphologies can be obtained in a controlled manner. The dissolution-electrodeposition processes were systematically investigated by cyclic voltammetry (CV), *in-situ* X-ray diffraction (XRD), *in-situ* Raman analysis, *etc.*, and the synthesized Ti_5Si_3 products were characterized by electron backscattered diffraction (EBSD), transmission electron microscopy (TEM), three-dimensional atomic probe (3DAP), *etc.* The results show that the morphology of the products can be significantly influenced by current density. By controlling current density at the range from 10 to 25 mA cm^{-2}, Ti_5Si_3 products with different morphologies, *i.e.*, dendritic particles, dense films, and porous powders, can be obtained in a controlled manner. Besides, Ti, Si atoms uniformly distributed in the films. The reaction mechanism of the formation of Ti_5Si_3 film was also proposed, which can be summarized as three periods: CaO-assisted dissolution of SiO_2 and TiO_2, the electrodeposition of Si and Ti, and the formation of stable Ti_5Si_3 phase. The CaO-assisted dissolution-electrodeposition process may provide a promising strategy for the production of Ti_5Si_3 alloy films and powders.

I. INTRODUCTION

WITH the development of modern science and technology, silicides with a high melting point have become a hotspot in the field of high-temperature structural materials, which are widely used in the national defense and industrial fields. Among these silicides (such as $TiSi_2$, NiSi, Ti_5Si_3, and CoSi), Ti_5Si_3 acts as a typical silicon intermetallic compound in the Ti-Si binary system,[1] as shown in Figure 1, and has received a tremendous amount of attention due to its distinct properties such as low density (4.32 g cm^{-3}), low electrical resistivity (50 to 120 $\mu\Omega$ cm), high melting point (2130 °C), excellent oxidation resistance, and high specific strength.[2–10] In addition to the preceding ideal performances, Ti_5Si_3 also has high hardness, unique chemical composition, and strong covalent bond, which causes it to potentially be regarded as a wear-resistant and corrosion-resistant coating material.[11]

Based on these excellent properties and bright application prospects, many researchers have tried to prepare Ti_5Si_3 intermetallic compounds by various methods. However, previous studies about the synthesis of Ti_5Si_3 mainly focused on conventional methods, including self-propagating high-temperature synthesis, mechanical alloying, and spark plasma sintering.[5–7,12–16] Most of these methods involve a process of arc melting of the ultrapure elements Ti and Si, which are produced by energy intensive and tedious processes, respectively. To alleviate this problem, many recent works focused on the production of Ti_5Si_3 have been reported. Estruga *et al.*[17] reported a novel synthesis of Ti_5Si_3 nanoparticles (NPs) *via* the magnesio-reduction of TiO_2 and SiO_2 NPs in eutectic LiCl-KCl molten salts at 700 °C. Devyatkin *et al.*[18] successfully obtained Ti_5Si_3 powders on nickel cathodes through electrodeposition from the chloro-fluoride melts ($NaCl$-KCl-K_2SiF_6-K_2TiF_6). Peng *et al.*[19] also reported a novel method for preparing Ti_5Si_3 powders from Ti-bearing blast furnace slag, which provided a feasible route for the treatment of titanium-bearing blast furnace slag and the recovery of titanium resources. Jiao *et al.*[20] and our previous work[21–24] also reported the preparation of Ti_5Si_3

WEI TANG, GUANGSHI LI, ZHONGYA PANG, XIANGYU XU, KAI ZHU, QIAN XU, XINGLI ZOU, and XIONGGANG LU are with the State Key Laboratory of Advanced Special Steel & Shanghai Key Laboratory of Advanced Ferrometallurgy & School of Materials Science and Engineering, Shanghai University, 99 Shangda Road, Shanghai 200444, China. Contact e-mails: xinglizou@shu.edu.cn; luxg@shu.edu.cn
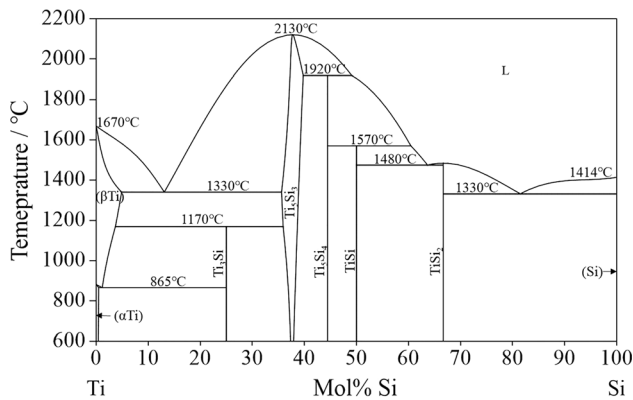
Fig. 1—Phase diagram of Ti-Si system, adapted from Ref. 1.

powders from their Ti/Si-containing metal oxide compounds using the Fray–Farthing–Chen Cambridge process and the solid oxide oxygen ion-conducting membrane-assisted electro-deoxidation process.

However, the methods mentioned previously can only produce Ti₅Si₃ powders other than dense films. It is still difficult to facilely produce dense crystalline Ti₅Si₃ films because of the high melting point of Ti₅Si₃. At present, Ti₅Si₃ films are mostly prepared by chemical vapor deposition and laser cladding.[2,25–27] These technologies have strict requirements on raw materials and the quality of the deposited products is hard to control. Therefore, searching for a cost-effective method is imminent at present.

In the present study, we report the successful demonstration of Ti₅Si₃ film electrodeposition in molten CaCl₂-CaO containing titanium/silicon dioxides at a relatively low temperature (850 °C). The method described here is similar to the pulse electrodeposition of TiB₂ thin films from fluoride melts.[28,29] The electrodeposition process was systematically investigated and the obtained Ti₅Si₃ products were characterized by electron backscattered diffraction (EBSD), transmission electron microscopy (TEM), three-dimensional atomic probe (3DAP), *etc*. Besides, the reaction mechanism for the electrodeposition of Ti₅Si₃ films was also proposed and discussed.

II. EXPERIMENTAL

A. *Solubility Test of TiO₂/SiO₂ in CaCl₂-CaO Melts at 850 °C*

The solubility test for the SiO₂ pellet was reported in the previous work and in our recent work.[30–33] In this work, the solubility test for TiO₂ is the same as for SiO₂. 2 g TiO₂ (99.5 pct, Sigma-Aldrich) powders were mixed with ~10 pct polyvinyl butyral by mechanical grinding, and then the milled mixture was pressed under 10 MPa to form a cylindrical pellet (15 mm in diameter and ~2 mm in thickness). The pellet was sandwiched by porous

nickel foil and then immersed in 100 g molten CaCl₂ (99 pct, Sigma-Aldrich) with the addition of 2 g CaO (99.9 pct, Sigma-Aldrich) at 850 °C for 24 hours. High-purity argon gas was continuously purged into the furnace during the entire process. Then the TiO₂ pellet was taken out from the molten salts and washed by distilled water. The immersed pellet was characterized by X-ray diffraction (XRD) spectroscopy. Besides, a small amount of molten salt was taken out from the crucible and diluted with deionized water. Then the diluted solution was detected by an inductively coupled plasma atomic emission spectrometer (ICP-AES, 7300DV) to determine the solubility of TiO₂ in molten CaCl₂-CaO.

B. *In-Situ XRD and In-Situ Raman Experiments*

In-situ XRD and *in-situ* Raman experiments were performed to analyze the dissolution processes for SiO₂ and TiO₂ in molten CaCl₂-CaO electrolyte. 0.1 g SiO₂ (99.5 pct, Sigma-Aldrich), 0.1 g TiO₂, 0.1 g CaO, and 0.3 g CaCl₂ were weighed and mixed. Then the mixed powders were placed upon a ceramic sieve (pore size of 0.2 mm) so that the high-purity argon gas could penetrate the sample and sample holder. This *in-situ* XRD experiment was performed using an X-ray powder diffractometer (Bruker D8 Advance, with Cu $K_{\alpha}1$ radiation). XRD patterns were collected at different temperatures (every 50 °C from 50 °C to 850 °C).

Before the *in-situ* Raman experiment, the sample (CaCl₂:CaO:SiO₂:TiO₂ = 30:2:1:1, mol pct) was mixed and then predissolved in a crucible at 850 °C. When cooled to 100 °C, the electrolyte sample was taken out and ground to a fine powder. The electrolyte sample was loaded into a platinum crucible for the *in-situ* Raman experiment and then heated from room temperature to 850 °C with a heating rate of 10 °C /min. It was recorded using a Horiba Jobin Y'von LabRAM HR Evolution laser confocal Raman spectrometer, which was equipped with an intensified charge coupled device detector and a hot stage (High-Temperature Observational System IRF-DP). A visible pulsed laser beam of 532 nm was used as an excitation source.

C. *Cyclic Voltammetry Measurements*

Cyclic voltammetry (CV) analysis was conducted to investigate the electrochemical behaviors of the electrolyte containing 100 g CaCl₂ with the addition of 2 g SiO₂, 2 g TiO₂, and 2 g CaO by using a three-electrode setup at 850 °C. Before the CV tests, the molten electrolyte was kept at 850 °C for 24 to 48 hours. The working electrode was a dense graphite plate (75-mm length × 2-mm width × 1-mm thickness). Graphite rods were employed as a counter electrode (6 mm in diameter) and a pseudo-reference electrode (3 mm in diameter), respectively. All electrodes were leaded by tungsten wires. More details about the CV experiment can be found in our previous work.[32,33]
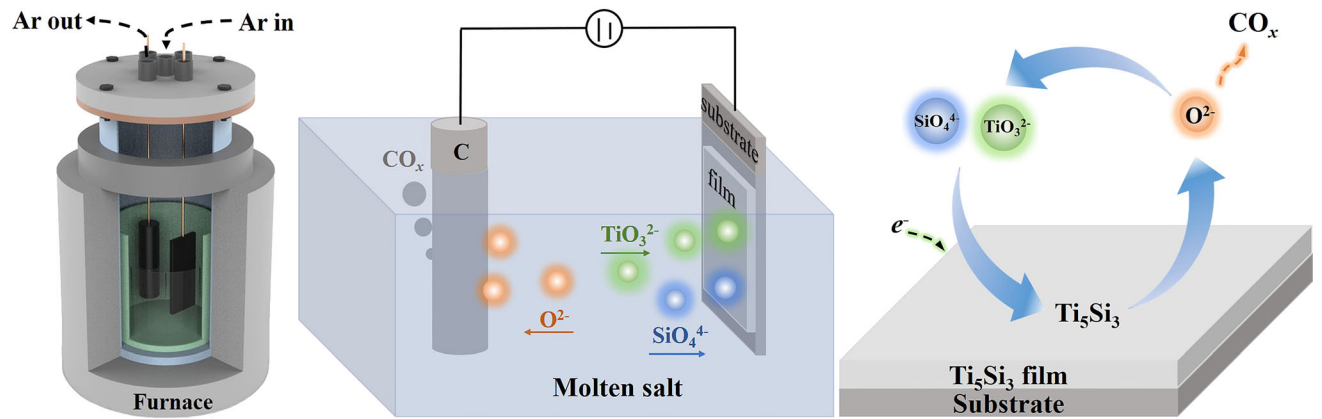
Fig. 2—Schematic illustrations of the electrodeposition of Ti_5Si_3 films in molten $CaCl_2$-CaO dissolved with SiO_2 and TiO_2 and the cyclic reaction mechanism.

D. *Molten Salt Electrodeposition Experiments*

A schematic diagram of the electrolytic cell for the electrodeposition of Ti_5Si_3 film is shown in Figure 2. In a typical experiment, 2 g SiO_2, 2 g TiO_2, and 2 g CaO were weighed and filled into a quartz crucible, and then 100 g $CaCl_2$ was placed into the crucible. CaO would act as a kind of cosolvent to accelerate the dissolution processes of TiO_2 and SiO_2. Subsequently, the crucible filled with these materials was put into a one-end close fused quartz tube in a furnace. The furnace was heated to 400 °C for 24 hours to make sure the possible water residual can be removed completely. And then the furnace was heated to 850 °C and kept at the temperature for 24 to 48 hours. During this period, pre-electrolysis was first carried out at 2.5 V for 12 to 24 hours between two graphite electrodes (graphite rod: 6-mm diameter × 50-mm length) to remove the possible impurities contained in the molten salts. After that, Ti_5Si_3 films were electrodeposited on a graphite substrate (graphite plate: 10-mm width × 50-mm length × 1-mm thickness) by applying pulse current density from 10 to 25 mA cm^{-2}, with a graphite rod as the anode. It should be noted that during the entire process, ultra-high-purity argon gas (99.999 pct) was continuously purged into the furnace to keep an inert atmosphere. After the electrolysis experiment, the deposited products were removed from the furnace and washed with tap water/distilled water as well as dried under vacuum.

E. *Materials Characterization*

The deposited products were characterized using XRD (Bruker-AXS D8 Advance), and the morphology of the synthesized films was examined by a scanning electron microscope (SEM, Quanta 650 FEG). The elemental composition was analyzed by an energy-dispersive X-ray spectroscope (EDS, XFlash Detector 5010) attached to the SEM. Before being analyzed by TEM (JEOL* 2100F) and 3DAP (LEAP 4000X HR), a

---

*JEOL is a trademark of JEOL, Tokyo.

dual beam focused ion beam (FIB, JEOL JIB-4500) was used to prepare the thin section out of Ti_5Si_3 film grown on the graphite substrate using the lift-out method. EBSD (Oxford Nordly max3) was also used to analyze the crystallographic orientation of deposited crystalline Ti_5Si_3.

III. RESULTS AND DISCUSSION

A. *Dissolution Behaviors of TiO_2/SiO_2 in Molten $CaCl_2$-CaO at 850 °C*

For the TiO_2 dissolution process, the solubility of TiO_2 in molten calcium chloride is generally low; however, the addition of CaO in molten $CaCl_2$ would also facilitate the dissolution process.[34,35] The use of CaO to enhance the solubility of TiO_2 in molten calcium chloride is similar to the previous work in fluorides.[36,37] In this work, the dissolution of TiO_2 in $CaCl_2$-CaO melts was determined by measuring the concentration of the titanium element in the melts. After the calculation, the solubility of TiO_2 in molten $CaCl_2$-2 wt pct CaO at 850 °C was determined to be approximately 0.43 mol pct by ICP analysis. The ICP results suggest that titanium oxides can dissolve in molten $CaCl_2$ with the addition of CaO, and the solubility of TiO_2 generally depends on the content of CaO dissolved in the molten $CaCl_2$.[34,35] In our previous work,[31,33] it was confirmed that SiO_2 would be converted into silicates ions (such as SiO_4^{4-}) in molten $CaCl_2$-CaO; then silicate ions could be reduced to form Si during electrodeposition. The solubility of SiO_2 in molten $CaCl_2$-CaO also generally depends on the content of CaO.[30] Thanks to the high solubility of CaO (~ 20 mol pct) in molten $CaCl_2$,[38] the solubility of SiO_2 in $CaCl_2$-2 wt pct CaO at 850 °C can be controlled at about 1.5 wt pct. It has been proved that the solubilities of TiO_2 and SiO_2 both increase with increasing temperature,[30,34,35] which implies that the solubilities of TiO_2 and SiO_2 can be controlled by varying the temperature and the CaO concentration in the molten salts. Accordingly, the tunable solubilities of SiO_2 and TiO_2 offer access to the direct electrodeposition of titanium silicides in molten $CaCl_2$-CaO.
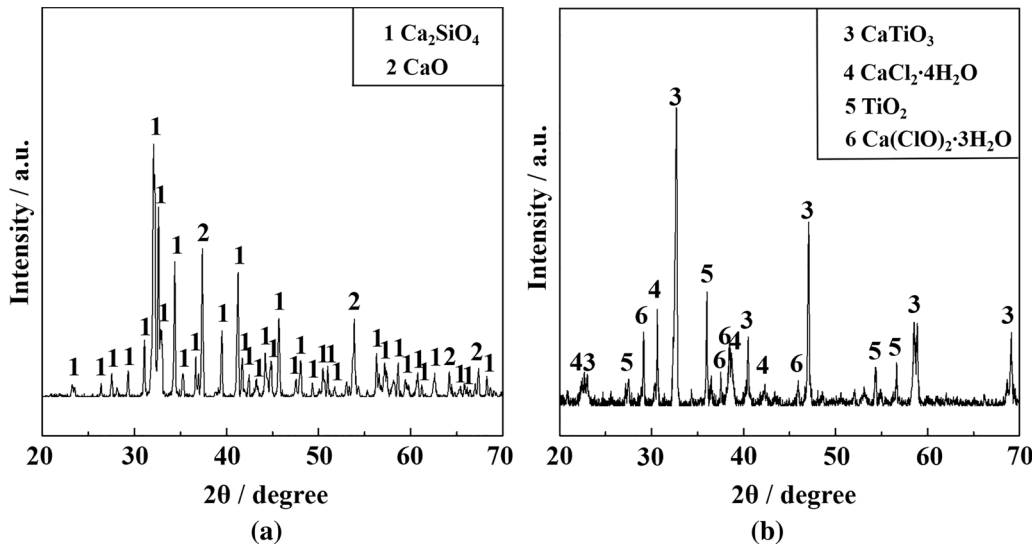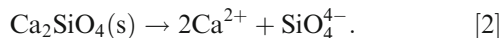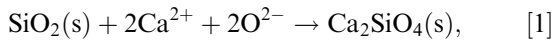
Fig. 3—XRD patterns of the (*a*) SiO_2 pellet and (*b*) TiO_2 pellet after being immersed in molten $CaCl_2$-CaO at 850 °C for 24 h.

In order to explore the dissolution behaviors of TiO_2/SiO_2 in molten $CaCl_2$ with the addition of CaO, the intermediate products of the TiO_2 and SiO_2 pellets after being immersed in molten $CaCl_2$-CaO at 850 °C for 24 hours were characterized by XRD, as shown in Figure 3. According to the results shown in Figure 3(a), only one calcium silicate (Ca_2SiO_4) appears on the SiO_2 pellet's surface after immersion, which is different from our assumption that various calcium silicates (such as $CaSiO_3$, Ca_2SiO_4, and $Ca_3Si_2O_7$) may be formed during the dissolution process. This finding indicates that Ca^{2+} and O^{2-} dissolved in molten $CaCl_2$ electrolyte would react with SiO_2 to form Ca_2SiO_4,[39] as expressed by Reaction [1]; then, Ca_2SiO_4 would dissolve into molten $CaCl_2$ to form SiO_4^{4-} (Reaction [2]).

$$SiO_2(s) + 2Ca^{2+} + 2O^{2-} \rightarrow Ca_2SiO_4(s), \qquad [1]$$

$$Ca_2SiO_4(s) \rightarrow 2Ca^{2+} + SiO_4^{4-}. \qquad [2]$$

Based on Figure 3(b), only one calcium titanate ($CaTiO_3$) is observed as the intermediate product on the surface of the TiO_2 pellet, which confirms that TiO_2 can react with Ca^{2+} and O^{2-} to form $CaTiO_3$,[40–42] as described by Reaction [3]. Then, $CaTiO_3$ would dissolve into the molten salts through Reaction [4]. It should be noted that Reactions [1] through [4] occur simultaneously during the dissolution process.

$$TiO_2 + Ca^{2+} + O^{2-} \rightarrow CaTiO_3, \qquad [3]$$

$$CaTiO_3 \rightarrow Ca^{2+} + TiO_3^{2-}. \qquad [4]$$
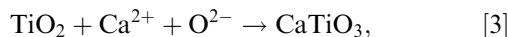
B. *Electrochemical Characteristics of the Process*

The CV curve of the electrodeposition process in molten $CaCl_2$-CaO containing SiO_2 and TiO_2 is shown in Figure 4(a). It can be seen that three reduction peaks and two oxidation peaks appeared. Peaks A1 and C1 at around 0/–0.6 V are mainly attributed to the reduction of Ca^{2+} and the dissolution of Ca, respectively. Peak C3 at approximately 0.75 V is attributed to the reduction of silicate ions.[31] During the dissolution process, CaO would dissolve into molten $CaCl_2$ to form Ca^{2+} and O^{2-} and then O^{2-} would react with SiO_2 to form SiO_4^{4-}. SiO_4^{4-} was reduced to silicon at a potential of approximately 0.75 V, as confirmed in our previous work.[31,33] Compared to the CV curve obtained in molten $CaCl_2$-CaO dissolved only SiO_2,[31] it is obvious that the peak C2 can be ascribed to the reduction of titanate ions. Accordingly, peak A2 starting at 0.5 V is the oxidation peak of the formed silicide $TiSi_x$. Based on the CV analysis, it is believed that TiO_2 particles would also react with CaO (Ca^{2+}, O^{2-}) to form titanate ions, *i.e.*, TiO_3^{2-}; then, the titanate ions can be reduced to Ti through electrodeposition.[34,35] The detailed reaction mechanisms, including the dissolution and the electrodeposition processes, will be discussed and summarized later. In this work, the pulse electrodeposition process (15 seconds at a current density of 10 to 25 mA cm^{-2} for electrodeposition and then 5 seconds at a current density of 0 mA cm^{-2} for the depletion layer to recover and bring ions to the electrode surface) was used to deposit $TiSi_x$ films. Figure 4(b) presents the typical potential-time curves of the pulse electrodeposition process, which shows a relatively stable electrodeposition process. Commonly, excessive TiO_2 and SiO_2 can be added into the molten $CaCl_2$-CaO, and these excessive TiO_2 and SiO_2 would remain at the bottom of the electrolytic cell. When the TiO_2/SiO_2 dissolved in $CaCl_2$ is consumed, the excess TiO_2/SiO_2 remaining at the bottom could be continuously dissolved. Therefore,
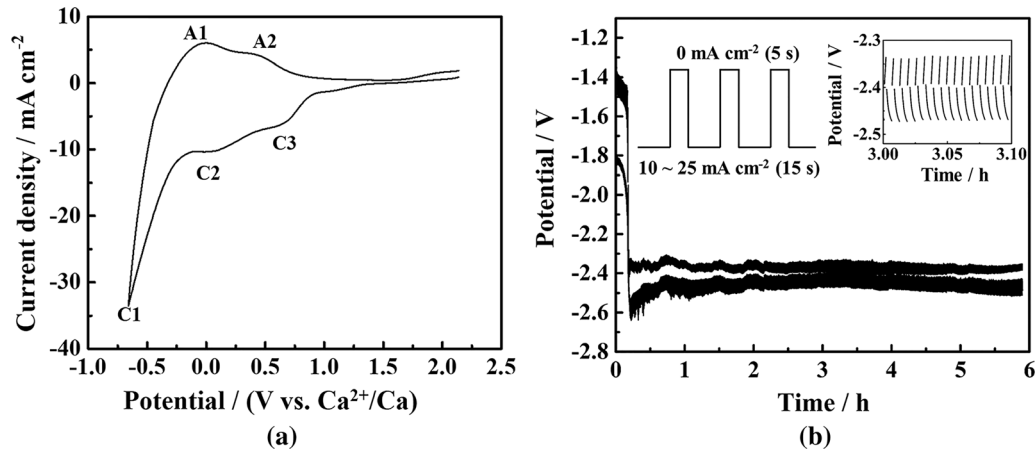
Fig. 4—(a) CV curve of the molten $CaCl_2$-CaO dissolved with TiO_2 and SiO_2 at 850 °C with a scan rate of 50 mV s^{-1}. (b) Typical potential-time curve of the pulse electrodeposition process for the production of Ti_5Si_3 films; the insets are the detailed conditions and partial plots.
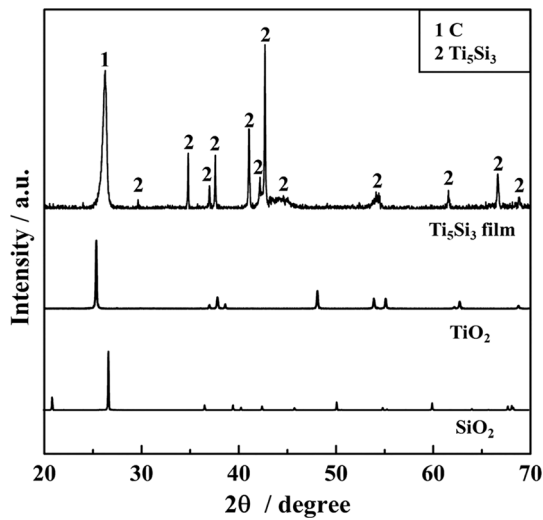

Fig. 5—XRD patterns of TiO_2, SiO_2 precursors, and the Ti_5Si_3 film deposited at 850 °C for 3 h with a current density of 15 mA cm^{-2}.

the dissolution and electrodeposition processes happen simultaneously, which means that the electrodeposition process is a continuous production process. Actually, continuous production of silicon through the dissolution-electrodeposition processes was demonstrated in our recent work.[43]

C. Characterization of the Ti-Si Products

The deposited Ti-Si films were analyzed using XRD, as shown in Figure 5. The result shows that the Ti-Si film is Ti_5Si_3 (JCPDS: 08-0041), and the lattice constants of Ti_5Si_3 can also be determined (a = 7.429 Å, c = 5.139 Å). Besides, the appearance of carbon peak is due to the graphite substrate. For comparison, the typical XRD patterns of the starting raw materials (TiO_2 and SiO_2) are also presented in Figure 5. It is evident that crystalline Ti_5Si_3 has been successfully produced from molten $CaCl_2$-CaO dissolved with TiO_2 and SiO_2 by using pulse electrodeposition. The Ti_5Si_3 deposited at

the current density of 15 mA cm^{-2} was also characterized by SEM and EDS analyses, as shown in Figure 6. It is evident that Ti_5Si_3 films with different thicknesses were deposited on the graphite substrate (Figures 6(a) through (c)) by changing the electrodeposition time, and the thickness of Ti_5Si_3 films can reach about 20 μm within 7 hours, as shown in Figure 6(c). It is suggested that the thickness and micromorphology of the film can be controlled by changing the current density, electrodeposition time, etc. Figures 6(d) through (f) are the elemental maps of the SEM image shown in Figure 6(c). The EDS mappings show that Ti, Si elements are uniformly distributed in the films, which further confirms the formation of Ti_5Si_3 film on the graphite substrate. Besides, the surface morphology observations (Figures 6(g) through (i)) further demonstrate that the crystal size of the deposited films can be controlled by changing the deposition time. At the beginning, the size of grains is not uniform, as shown in Figure 6(g). When the electrodeposition time reaches 3 hours, dense film gradually forms and the grains become more homogeneous.

In order to further characterize the deposited Ti_5Si_3 film, 3DAP analysis was performed. Figure 7 presents the elemental distribution of Ti and Si atoms in the Ti_5Si_3 film deposited at 15 mA cm^{-2} for 3 hours. It can be seen that Ti and Si elements are uniformly distributed in the Ti_5Si_3 film. To understand the growth process and crystal orientation of the deposited Ti_5Si_3 film, EBSD analysis was also performed. Figure 8(a) shows the SEM image of the scanning area. Based on the EBSD analysis result, it can be seen that equiaxed grains with a random orientation start to deposit on the graphite substrate during the initial period (Figures 8(b) and (c)). Gradually, the grains show a preferred orientation with a fiber texture of (0001) along the normal direction and present a long column (Figures 8(b) through (d)), which is similar to the solidification behavior of columnar crystals. The misorientation angle distribution in Figure 8(e) also reveals that there are many low-angle grain boundaries with grain misorientations less than 5 deg, and high-angle grain boundaries are mainly distributed under 45 deg, which results from the fiber texture.
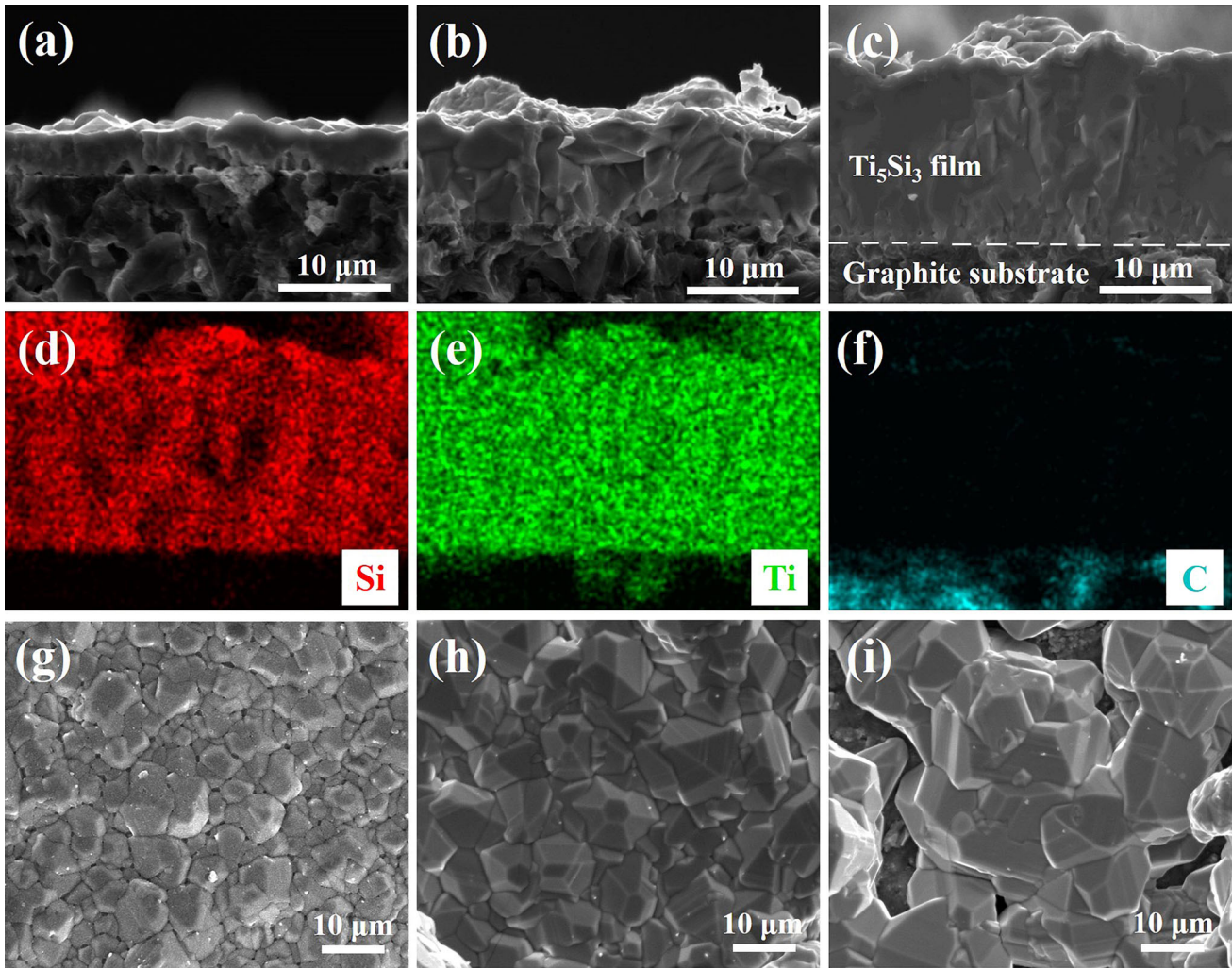
Fig. 6—SEM images of the cross sections of the Ti_5Si_3 films obtained at 850 °C for (a) 1 h, (b) 3 h, and (c) 7 h with a current density of 15 mA cm^{-2}; (d) through (f) corresponding EDS elemental mappings over the image (c); (g) through (i) SEM images of the surfaces of the Ti_5Si_3 films obtained at 850 °C for 1, 3, and 7 with a current density of 15 mA cm^{-2}, respectively.
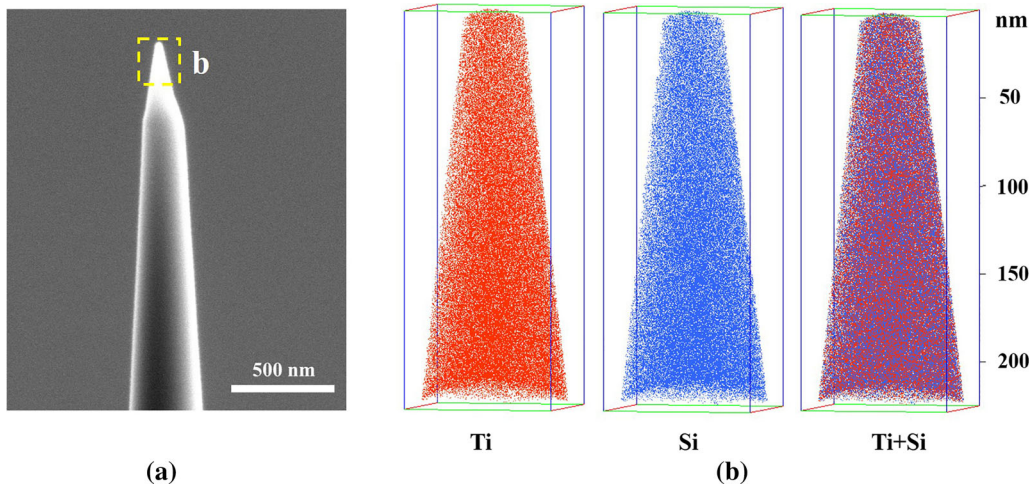

Fig. 7—(a) SEM image of the 3DAP needle specimen and (b) 3DAP maps of Ti, Si, elements of Ti_5Si_3 film deposited at 15 mA cm^{-2}.
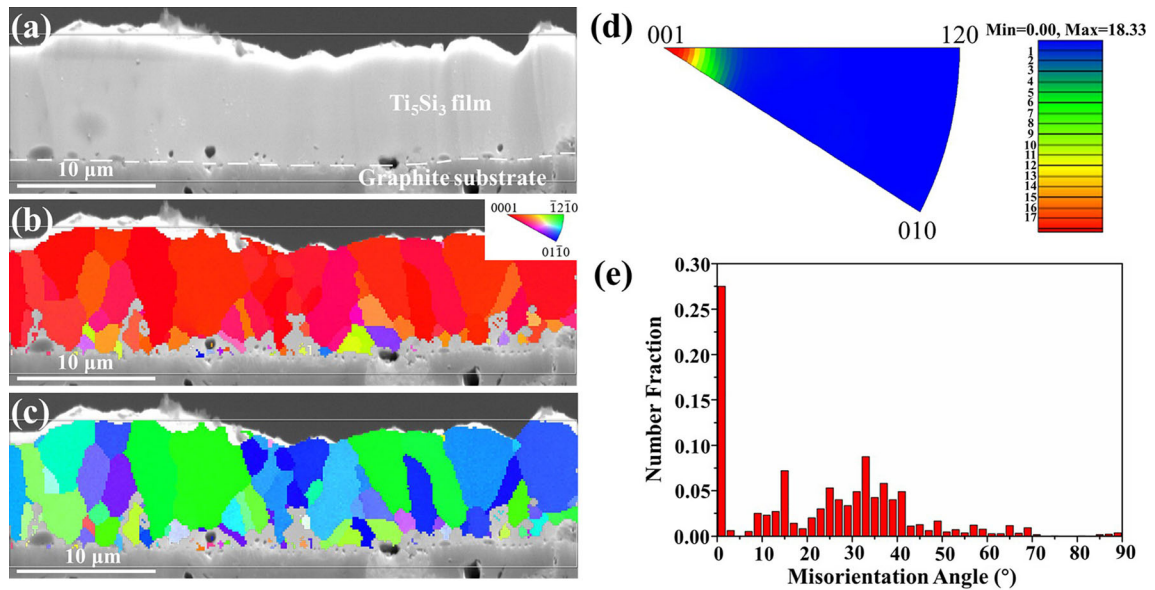
Fig. 8—(*a*) SEM image of the cross section for the Ti_5Si_3 film deposited at 15 mA cm^{-2} for 3 h; (*b*) corresponding inverse pole figure (IPF)-Y (normal direction) and (*c*) IPF-Z; (*d*) distribution of orientation along the normal direction; and (*e*) fraction of misorientation angles for the microstructure of Ti_5Si_3 in (a).

Except Ti_5Si_3 film, Ti_5Si_3 powders can also be produced by electrodeposition. Figure 9 displays the SEM images of products obtained at different current densities. Figure 9(a) shows the SEM image of the surface of Ti_5Si_3 film deposited at 15 mA cm^{-2} for 3 hours and its corresponding elemental mappings. Apparently, Ti and Si elements are distributed uniformly on the surface. When the current density increases to 25 mA cm^{-2}, the nucleation rate increases; thus, porous Ti_5Si_3 powders are formed. On the contrary, when the current density decreases to 10 mA cm^{-2}, the nucleation rate decreases and the formed nuclei have sufficient time to grow to form dendritic particles, as shown in Figure 9(c). In this work, the current efficiency for the electrodeposition of Ti_5Si_3 film is hard to accurately calculate because a small amount of powders would be generated on the surface of Ti_5Si_3 films. However, according to our previous work[31–33] and based on the similar experimental observations, the current efficiencies for the electrodeposition of Ti_5Si_3 products at 10, 15, and 25 mA cm^{-2} are believed to be approximately 50 to 60 pct.

The typical Ti-Si products deposited on graphite substrate were then analyzed by TEM, and the TEM images are shown in Figures 10(a) through (d). Figure 10(a) and (c) are the high-resolution TEM (HRTEM) images, while Figures 10(b) and (d) are their corresponding FFT diffraction patterns. The FFT image in Figure 10(b) displays typical features of an equilateral triangle, which matches a [001] crystal belt axis diffraction pattern. According to the crystal interplanar spacing marked in Figure 10(a), the lattice constant can be estimated to be 7.44 Å, which is consistent with the XRD results. Figure 10(c) shows the characteristic spacings of 0.627, 0.402, and 0.399 nm for the (0$\bar{1}$0), (101), and (1$\bar{1}$1) lattice planes (Figure 10(d)). It can be

inferred from Figure 10(c) that the lattice constants are 7.44 Å and 5.114 Å, which also agree with the XRD results. Thus, a hexagonal Ti_5Si_3 compound ($P63/mcm$) was confirmed and its crystal structure is inserted in Figure 10(d).

D. *Reaction Mechanisms*

As expected, Ti_5Si_3 films have been directly electrodeposited from molten $CaCl_2$-CaO dissolved with TiO_2 and SiO_2. Based on the experimental results and the previous studies,[30,33,34] the general reaction mechanism of the electrodeposition of Ti_5Si_3 can be summarized as three periods: (1) CaO-assisted dissolution of SiO_2 and TiO_2 in molten $CaCl_2$ to form silicate ions (SiO_4^{4-}) and titanate ions (TiO_3^{2-}), respectively; (2) electrodeposition of Si and Ti from silicate ions and titanate ions, respectively; and (3) formation of stable Ti_5Si_3 through Si, Ti → $TiSi_2$ → Ti_5Si_3.

(1) It has been proved that the addition of CaO can promote the dissolution of SiO_2 and TiO_2 in molten $CaCl_2$.[30,35] To reveal the CaO-assisted dissolution process more intuitively, *in-situ* XRD analysis and an *in-situ* Raman experiment were performed to explore the phase transformation during the dissolution process. Figure 11(a) plots the accumulated *in-situ* XRD data collected during the process. When the temperature is below 400 °C, the phase composition does not change. With the increase of temperature, Ca_4OCl_6 begins to appear. When the temperature reaches about 750 °C or higher, the peaks of SiO_2, TiO_2, and CaO disappear and Ca_2SiO_4, $Ca_3SiO_4Cl_2$, and $CaTiO_3$ appear, which is consistent with the preceding results. Based on these results, the main chemical reactions that occurred during the entire heating process can be seen in Figure 11(b).
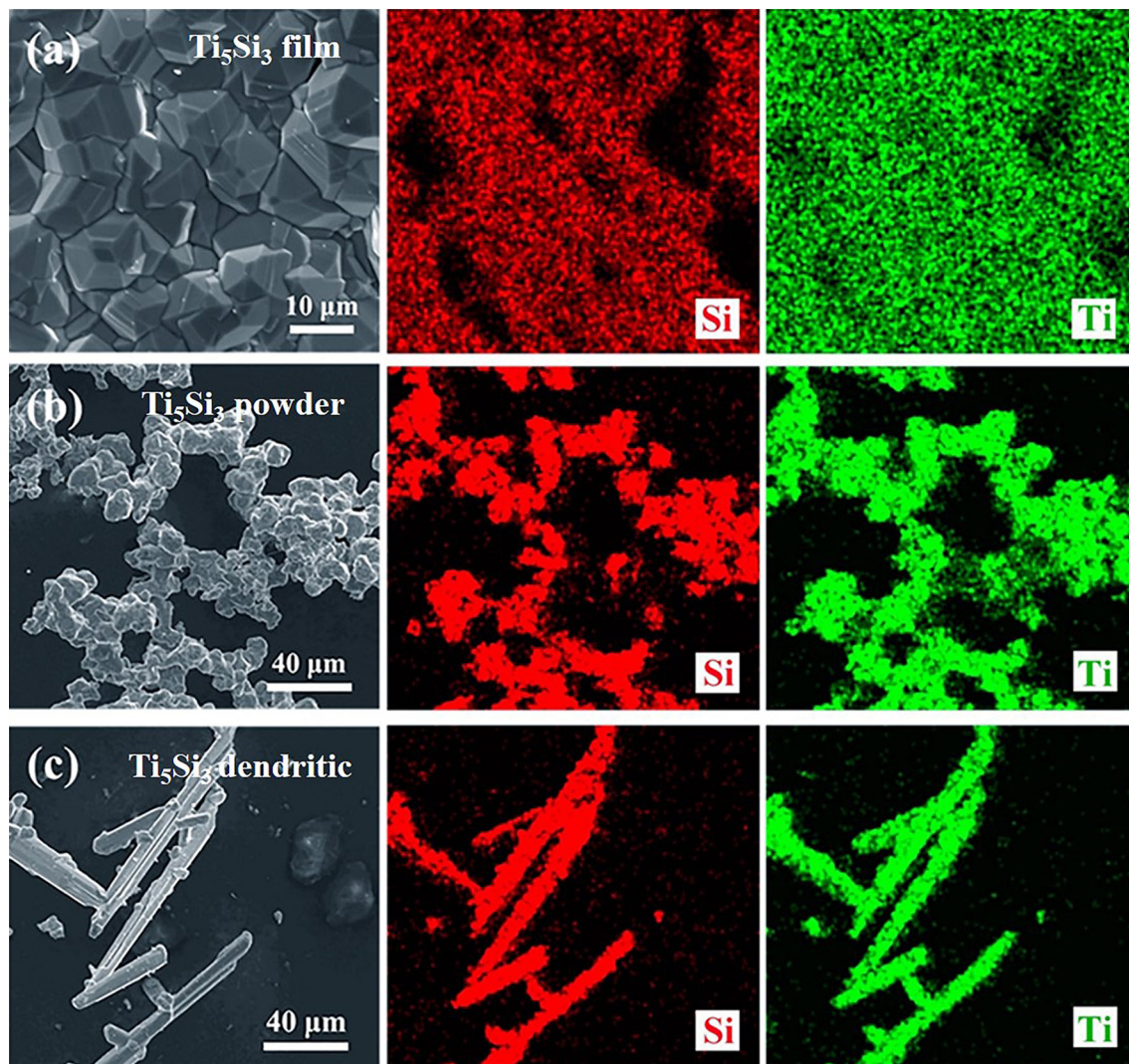
Fig. 9—SEM images and their corresponding EDS elemental mappings of the Ti_5Si_3 products deposited at 850 °C for 3 h at different current densities: (*a*) 15 mA cm^{-2}, (*b*) 25 mA cm^{-2}, and (*c*) 10 mA cm^{-2}.

Figure 12 shows the *in-situ* high-temperature Raman spectra and their corresponding fitting results. Based on previous studies,[44–46] the Raman peaks in Figures 12(a) and (b) correspond to $[TiO_3]^{2-}$ and $[SiO_4]^{4-}$, respectively, which is consistent with the *in-situ* XRD results (Figure 11). When adding SiO_2 and TiO_2 into the molten $CaCl_2$-CaO simultaneously, the silicate ions and titanate ions coexist in the molten salts, as shown in Figure 12(c). The Raman peaks at 160, 223, 280, 337, 673, and 797 cm^{-1} in Figure 12(c) are assigned to $[TiO_3]^{2-}$. The vibrational modes of 223, 280, and 337 cm^{-1} are associated with the O-Ti-O bending vibrations.[47] The Raman peak 673 cm^{-1} originates from the Ti-O symmetrical vibrations.[44] Besides, the remaining peaks at 443 and 979 cm^{-1} are related to $[SiO_4]^{4-}$.[48] These results indicate that CaO can accelerate the dissolution processes for SiO_2 and TiO_2 in molten $CaCl_2$.

(2) After 24 to 48 hours of the dissolution process at 850 °C, sufficient silicate ions and titanate ions are formed and dissolved in the $CaCl_2$ melt. When a pulse current is applied, these silicate ions and titanate ions around the cathode are electroreduced to Si and Ti metals, respectively, and the related electrochemical reactions are listed as Reactions [5] and [6]. Figure 13 shows the XRD result of the products collected from the graphite cathode when applying a pulse current of 25 mA cm^{-2} for 0.5 hours. It can be seen that silicon is formed during this process, which suggests that silicate ions would be reduced to form silicon prior to the electroreduction of titanate ions. Although no titanium is observed, the lower oxide Ti_5O_9 appears; this observation is similar to the report of Suzuki.[49] It is suggested that the reduction of titanate ions involves a multistep reaction process in the $CaCl_2$ melt (Reactions [7] and [8]), which is consistent with the previous work.[22,50]
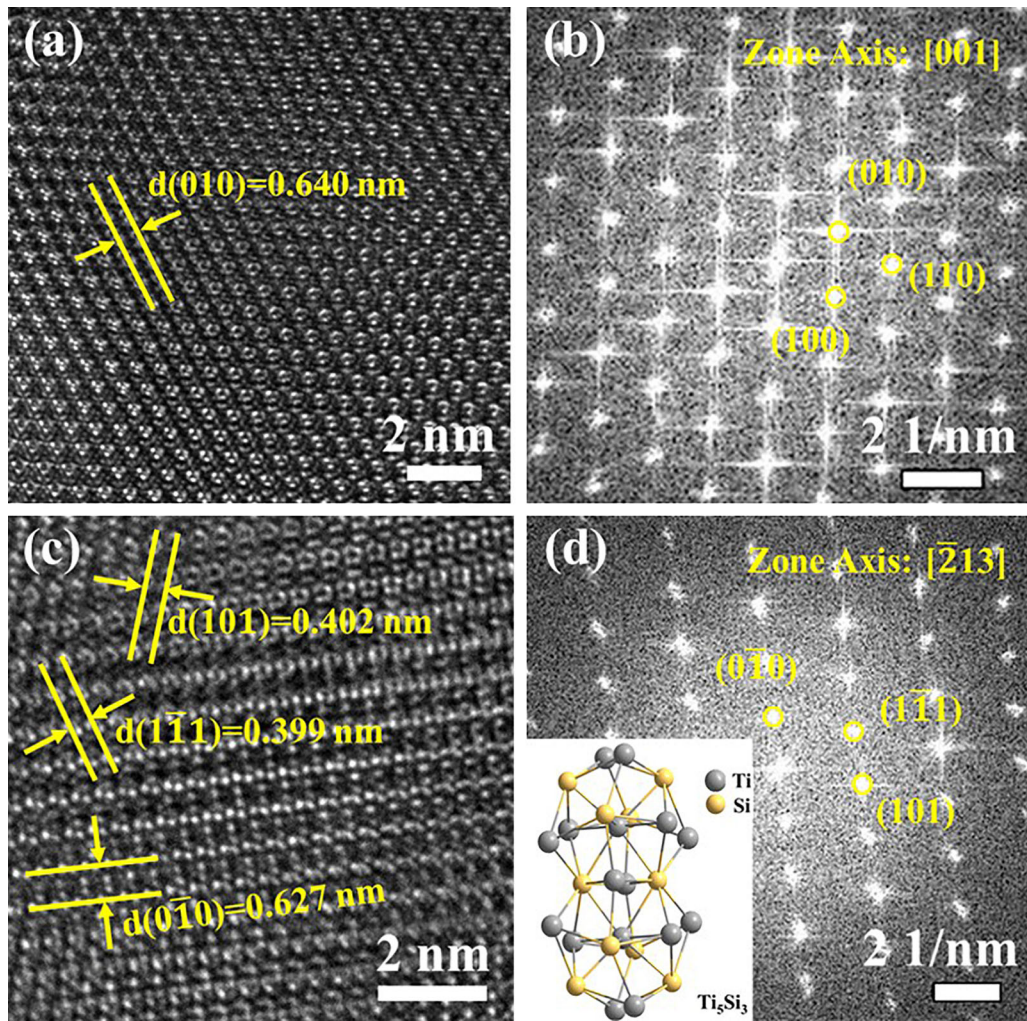
Fig. 10—(*a*) and (*c*) HRTEM images of the Ti_5Si_3 film electrodeposited at 850 °C for 3 h; (*b*) and (*d*) corresponding SAED patterns of (a) and (c). The inset in (d) is the crystal structure of Ti_5Si_3.
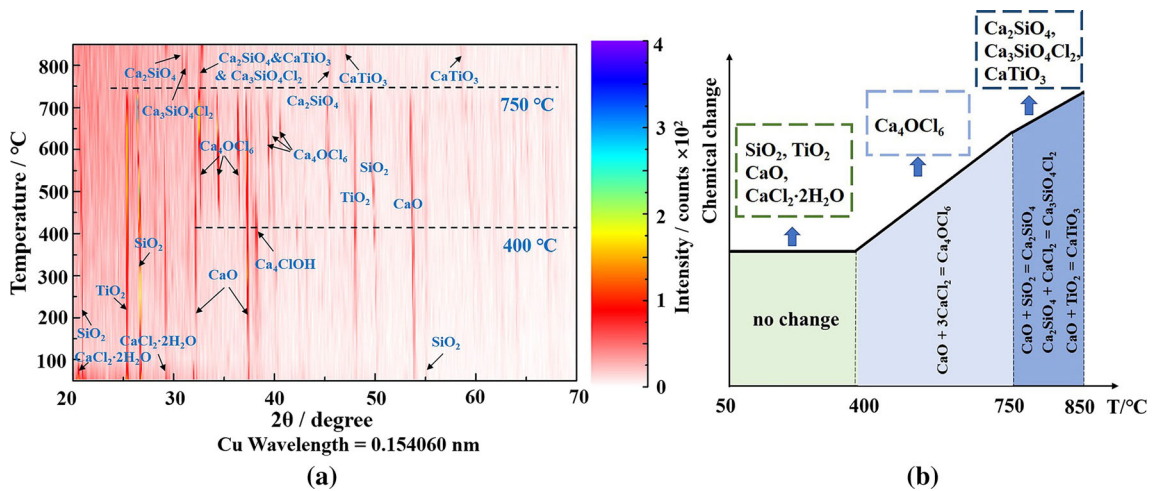

Fig. 11—(*a*) *In-situ* XRD data collected for the mixture of SiO_2, TiO_2, CaO, and $CaCl_2$ at different temperatures (every 50 °C from 50 °C to 850 °C, with a heating rate of 5 °C/min) under argon atmosphere, respectively; (*b*) the possible reaction mechanism of the heating process.
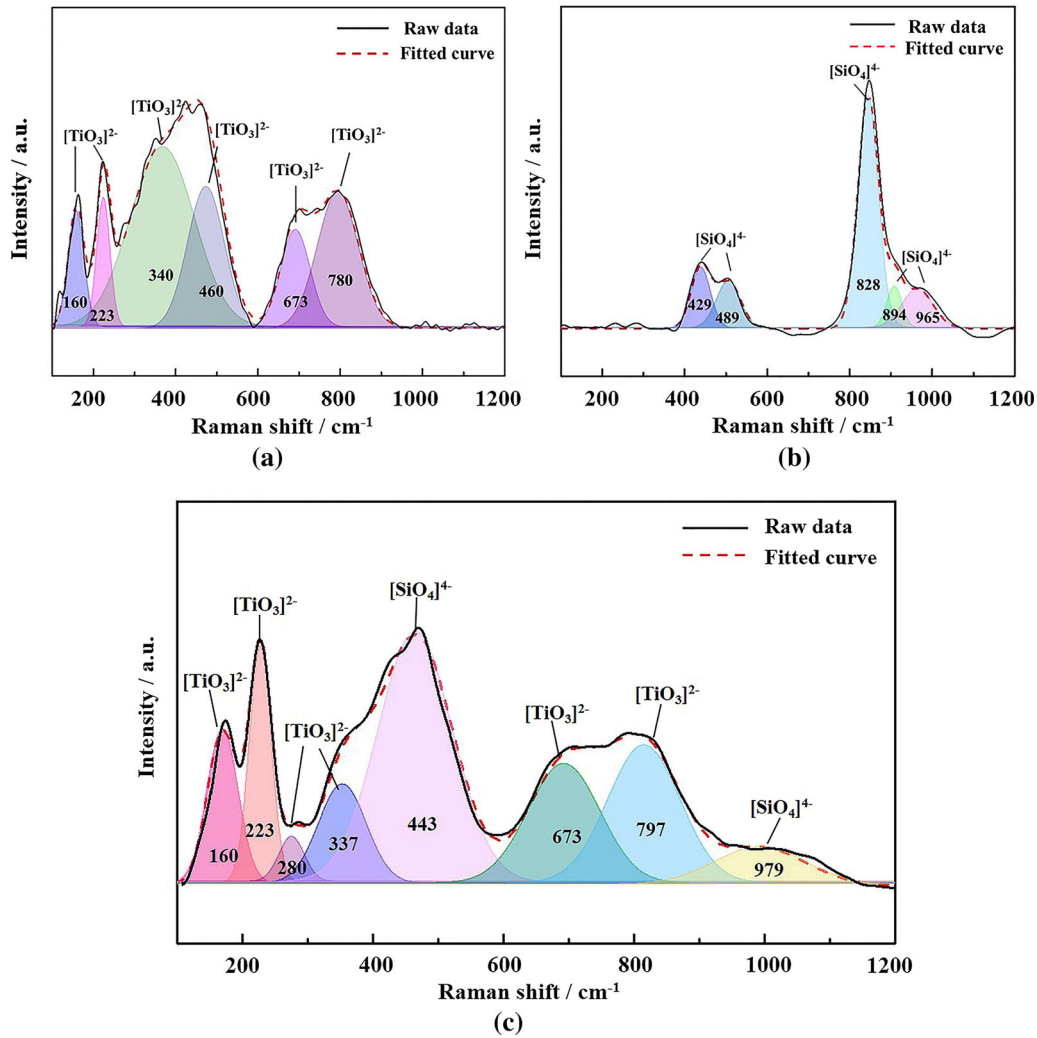
Fig. 12—*In-situ* high-temperature Raman spectra collected from (*a*) CaCl$_2$-CaO-TiO$_2$, (*b*) CaCl$_2$-CaO-SiO$_2$, and (*c*) CaCl$_2$-CaO-TiO$_2$-SiO$_2$ at 850 °C under argon atmosphere.
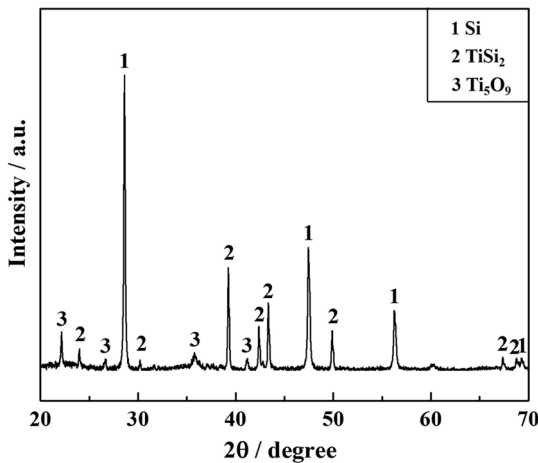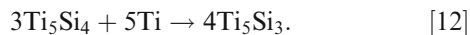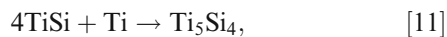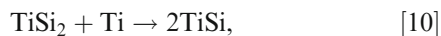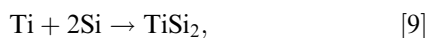

Fig. 13—Typical XRD pattern of the deposited Ti-Si film collected from the graphite substrate after applying a pulse current of 25 mA cm^{-2} for 0.5 h.

$$SiO_4^{4-} + 4e^- \rightarrow Si + 4O^{2-}, \quad [5]$$

$$TiO_3^{2-} + 4e^- \rightarrow Ti + 3O^{2-}, \quad [6]$$

$$5TiO_3^{2-} + 2e^- \rightarrow Ti_5O_9 + 6O^{2-}, \quad [7]$$

$$Ti_xO_{(2x+y)}^{2y-} + 4xe^- \rightarrow xTi + (2x+y)O^{2-}. \quad [8]$$
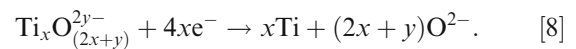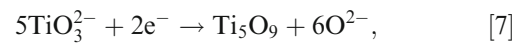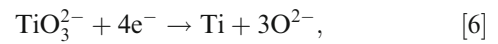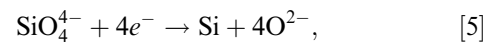
(3) The electrodeposited titanium and silicon would react with each other to form various kinds of titanium-silicon silicides (Reactions [9] through [12]), such as TiSi, TiSi$_2$, Ti$_5$Si$_3$, and Ti$_5$Si$_4$.[18,51] With prolonged time, Ti$_5$Si$_3$ finally would be obtained (Si, Ti $\rightarrow$ TiSi$_2$ $\rightarrow$ Ti$_5$Si$_3$) because of its excellent sta-

bility among the titanium silicides,[52] which was also discussed in our previous studies.[22]

$$Ti + 2Si \rightarrow TiSi_2, \qquad [9]$$

$$TiSi_2 + Ti \rightarrow 2TiSi, \qquad [10]$$

$$4TiSi + Ti \rightarrow Ti_5Si_4, \qquad [11]$$

$$3Ti_5Si_4 + 5Ti \rightarrow 4Ti_5Si_3. \qquad [12]$$

It is noteworthy that during the entire process, the formation steps mentioned previously are not necessarily in a chronological order; they can occur simultaneously during the electrodeposition process. When silicate ions and titanate ions in the molten salts are reduced to Si and Ti, the continuous dissolution process takes place accordingly and the dissolution-electrodeposition processes proceed simultaneously. We note that the reaction mechanism can only be considered as a general guideline to understand the electrodeposition process; further investigation is currently being undertaken.

IV. CONCLUSIONS

We have demonstrated that Ti_5Si_3 films can be successfully electrodeposited in molten $CaCl_2$-CaO dissolved with TiO_2 and SiO_2 at a relatively low temperature (850 °C) by applying pulse current. The morphology of the products can be significantly influenced by current density. By controlling current density at the range from 10 to 25 mA cm^{-2}, Ti_5Si_3 products with different morphologies, i.e., dendritic particles, dense films, and porous powders, can be obtained in a controlled manner. Besides, Ti, Si atoms uniformly distributed in the films. The mechanism of the formation of Ti_5Si_3 film can be divided into three periods: (1) CaO-assisted dissolution of SiO_2 and TiO_2 in molten $CaCl_2$ to form silicate ions and titanate ions, respectively; (2) electrodeposition of Si and Ti from silicate ions and titanate ions, respectively; (3) formation of stable Ti_5Si_3 through Si, Ti $\rightarrow TiSi_2 \rightarrow Ti_5Si_3$. The CaO-assisted dissolution-electrodeposition strategy may have great potential to be used for the production of refractory Ti_5Si_3 alloy films or powders. This strategy may also have implications for the production of other refractory alloys.

ACKNOWLEDGMENTS

REFERENCES

1. T.B. Massalski, P.R. Subramanian, H. Okamoto, and L. Kacprzak: *Binary Alloy Phase Diagrams*, 2nd ed., ASM International, Materials Park, OH, 1990.
2. Z. Ren, Y. Huang, M. Shen, C. Song, W. Weng, G. Han, N. Ma, and P. Du: *J. Non-Cryst. Solids*, 2011, vol. 357, pp. 2802–09.
3. K. Ito, T. Hayashi, and H. Nakamura: *Intermetallics*, 2004, vol. 12, pp. 443–50.
4. L. Zhang and J. Wu: *Acta Mater.*, 1998, vol. 46, pp. 3535–46.
5. K. Kasraee, M. Yousefpour, and S.A. Tayebifard: *J. Alloys Compd.*, 2019, vol. 779, pp. 942–49.
6. S. Li, X. Zou, K. Zheng, X. Lu, C. Chen, X. Li, Q. Xu, and Z. Zhou: *Metall. Mater. Trans. B*, 2018, vol. 49B, pp. 790–802.
7. W.H. Lee, Y.W. Cheon, Y.H. Yoon, C.H. Jeong, C.J. Van Tyne, and H.G. Lee: *Int. J. Refract. Met. Hard Mater.*, 2019, vol. 80, pp. 174–80.
8. J.H. Schneibel and C.J. Rawn: *Acta Mater.*, 2004, vol. 52, pp. 3843–48.
9. S. Agarwal, E.J. Cotts, S. Zarembo, R. Kematick, and C. Myers: *J. Alloys Compd.*, 2001, vol. 314, pp. 99–102.
10. D. Szwagierczak: *Ceram. Int.*, 2004, vol. 30, pp. 757–64.
11. L. Liu, J. Xu, P. Munroe, and Z.-H. Xie: *Electrochim. Acta*, 2014, vol. 115, pp. 86–95.
12. C.L. Yeh, W.H. Chen, and C.C. Hsu: *J. Alloys Compd.*, 2007, vol. 432, pp. 90–95.
13. J. Liu, Y. Bai, P. Chen, N. Cui, and H. Yin: *J. Alloys Compd.*, 2013, vol. 555, pp. 375–80.
14. S.G. Vadchenko, A.E. Sytschev, D.Y. Kovalev, A.S. Shchukin, and A.F. Belikova: *Int. J. Self-Propag. High-Temp. Synth.*, 2014, vol. 23, pp. 141–44.
15. K. Kasraee, A. Tayebifard, and E. Salahi: *J. Mater. Eng. Perform.*, 2013, vol. 22, pp. 3742–48.
16. A. Calka, A.P. Radlinski, R.A. Shanks, and A.P. Pogany: *J. Mater. Sci. Lett.*, 1991, vol. 10, pp. 734–37.
17. M. Estruga, S.N. Girard, Q. Ding, L. Chen, X. Li, and S. Jin: *Chem. Commun.*, 2014, vol. 50, pp. 1454–57.
18. S.V. Devyatkin, O.I. Boiko, N.N. Uskova, and G. Kaptay: *Z. Naturforsch. A: Phys. Sci.*, 2001, vol. 56, pp. 739–40.
19. B. Peng, L. Wu, J.-H. Zhu, Y. Hou, and G.-H. Zhang: *Metall. Res. Technol.*, 2020, vol. 117, p. 614.
20. H. Jiao, Q. Wang, J. Ge, H. Sun, and S. Jiao: *J. Alloys Compd.*, 2014, vol. 582, pp. 146–50.
21. X. Zou, X. Lu, Z. Zhou, W. Xiao, Q. Zhong, C. Li, and W. Ding: *J. Mater. Chem. A*, 2014, vol. 2, pp. 7421–30.
22. X. Zou, X. Lu, Z. Zhou, C. Li, and W. Ding: *Electrochim. Acta*, 2011, vol. 56, pp. 8430–37.
23. X. Zou, X. Lu, Z. Zhou, and C. Li: *Electrochem. Commun.*, 2012, vol. 21, pp. 9–13.
24. X. Zou, X. Lu, C. Li, and Z. Zhou: *Electrochim. Acta*, 2010, vol. 55, pp. 5173–79.
25. D. Gu, J. Liu, G. Meng, C. Li, Y. Li, and Y. Shen: *Mater. Sci. Technol.*, 2011, vol. 27, pp. 1736–40.
26. D. Gu, Y. Shen, and Z.J.M.L. Lu: *Mater. Lett.*, 2009, vol. 63, pp. 1577–79.
27. D. Vojtech, P. Novak, P. Machac, A. Mort'anikova, and K. Jurek: *J. Alloys Compd.*, 2008, vol. 464, pp. 179–84.
28. L. Jun and L. Bing: *Mater. Lett.*, 2007, vol. 61, pp. 1274–78.
29. G. Ett and E.J. Pessine: *Electrochim. Acta*, 1999, vol. 44, pp. 2859–70.
30. W. Xiao, X. Wang, H. Yin, H. Zhu, X. Mao, and D. Wang: *RSC Adv.*, 2012, vol. 2, pp. 7588–93.
31. X. Zou, L. Ji, J. Ge, D.R. Sadoway, E.T. Yu, and A.J. Bard: *Nat. Commun.*, 2019, vol. 10, pp. 5772–79.
32. X. Zou, L. Ji, X. Yang, T. Lim, E.T. Yu, and A.J. Bard: *J. Am. Chem. Soc.*, 2017, vol. 139, pp. 16060–63.

33. X. Yang, L. Ji, X. Zou, T. Lim, J. Zhao, E.T. Yu, and A.J. Bard: *Angew. Chem., Int. Ed.*, 2017, vol. 56, pp. 15078–82.
34. T. Takenaka, K. Shimokawa, K. Nishikawa, H. Okada, and T. Morishige: *Mater. Trans.*, 2017, vol. 58, pp. 350–54.
35. H. Okada, K. Shimokawa, T. Morishige, and T. Takenaka: *Mater. Trans.*, 2018, vol. 59, pp. 690–93.
36. S. Su, T. Villalon, Jr., U. Pal, and A. Powell: *Proc. 10th Int. Conf. on Molten Slags, Fluxes and Salts (MOLTEN16)*, 2016, pp. 465–75.
37. J. Guo, T. Villalon, U. Pal, and S. Basu: *J. Am. Ceram. Soc.*, 2018, vol. 101, pp. 3605–16.
38. D.A. Wenz, I. Johnson, and R.D. Wolson: *J. Chem. Eng. Data*, 1969, vol. 14, pp. 250–52.
39. Y. Katasho, Y. Norikawa, T. Yamamoto, K. Yasuda, and T. Nohira: *Electrochem. Commun.*, 2020, vol. 115, art. no. 106740.
40. R. Bhagat, D. Dye, S.L. Raghunathan, R.J. Talling, D. Inman, B.K. Jackson, K.K. Rao, and R.J. Dashwood: *Acta Mater.*, 2010, vol. 58, pp. 5057–62.
41. M. Hu, T. Ma, L. Gao, P. Lai, Z. Qu, L. Wen, D. Li, S. Zhang, and M. Hu: *Mater. Trans.*, 2019, vol. 60, pp. 416–21.
42. G.Z. Chen and D.J. Fray: *J. Electrochem. Soc.*, 2002, vol. 149, p. 455.
43. X. Zou, L. Ji, Z. Pang, Q. Xu, and X. Lu: *J. Energy Chem.*, 2020, vol. 44, pp. 147–53.
44. F. Shi, G.E. Fu, E.C. Xiao, and J. Li: *J. Mater. Sci.: Mater. Electron.*, 2020, vol. 31, pp. 18070–76.
45. H. Zheng, I.M. Reaney, G.D.C. Csete de Györgyfalva, R. Ubic, J. Yarwood, M.P. Seabra, and V.M. Ferreira: *J. Mater. Res.*, 2004, vol. 19, pp. 488–95.
46. M.L. Moreira, E.C. Paris, G.S. do Nascimento, V.M. Longo, J.R. Sambrano, V.R. Mastelaro, M.I.B. Bernardi, J. Andrés, J.A. Varela, and E. Longo: *Acta Mater.*, 2009, vol. 57, pp. 5174–85.
47. U. Balachandran and N.G. Eror: *Solid State Commun.*, 1982, vol. 44, pp. 815–18.
48. C. Remy, B. Reynard, and M. Madon: *J. Am. Ceram. Soc.*, 1997, vol. 80, pp. 413–23.
49. R.O. Suzuki, K. Ono, and K. Teranuma: *Metall. Mater. Trans. B*, 2003, vol. 34B, pp. 287–95.
50. D.T.L. Alexander, C. Schwandt, and D.J. Fray: *Electrochim. Acta*, 2011, vol. 56, pp. 3286–95.
51. J. Trambukis and Z.A. Munir: *J. Am. Ceram. Soc.*, 1990, vol. 73, pp. 1240–45.
52. Y.J. Du, K.P. Rao, J.C.Y. Chung, and X.D. Han: *Metall. Mater. Trans. A*, 2000, vol. 31A, pp. 763–71.